BioDrugs (2020) 34:77–87
https://doi.org/10.1007/s40259-019-00390-1

ORIGINAL RESEARCH ARTICLE

Crystal Structures of PF-06438179/GP1111, an Infliximab Biosimilar

Thomas F. Lerch[1] · Penelope Sharpe[2] · Stephen J. Mayclin[3] · Thomas E. Edwards[3] · Sharon Polleck[2] · Jason C. Rouse[2] · Qin Zou[1] · Hugh D. Conlon[2]

Published online: 24 October 2019

Abstract

Background Higher-order structure (HOS) assessment is an important component of biosimilarity evaluations. While established spectroscopic methods are routinely used to characterize structure and evaluate similarity, the addition of X-ray crystallographic analysis to these biophysical methods enables orthogonal elucidation of HOS at higher resolution.

Methods Crystal structures of the infliximab biosimilar PF-06438179/GP1111 and the reference product Remicade®, sourced from US and European Union markets, were determined and compared to evaluate HOS similarity. Analytical ultracentrifugation studies were conducted to understand reversible self-association.

Results In contrast to more routine spectroscopic methods, the crystal structures enable three-dimensional assessment of complementarity-determining regions and other local regions at near-atomic resolution. The biosimilar structures are highly similar to those of the reference product, as demonstrated visually and though all-atom root-mean-squared deviation measurements.

Conclusion The structures provide new insights into the physicochemical properties of the proposed biosimilar and the reference product, further strengthening the 'totality of evidence' in the evaluation of similarity.

Key Points

The first crystal structures of an infliximab biosimilar are presented.

Crystallography enables site-specific structural detailing of regions important for the physicochemical and functional properties of infliximab.

The structures support the demonstration of biosimilarity to the reference product, Remicade®.

Electronic supplementary material The online version of this article (https://doi.org/10.1007/s40259-019-00390-1) contains supplementary material, which is available to authorized users.

✉ Thomas F. Lerch
thomas.lerch@pfizer.com

Penelope Sharpe
penny.sharpe@pfizer.com

Stephen J. Mayclin
smayclin@be4.com

Thomas E. Edwards
tedwards@be4.com

Sharon Polleck
sharon.polleck@pfizer.com

Jason C. Rouse
jason.rouse@pfizer.com

Qin Zou
qin.zou@pfizer.com

Hugh D. Conlon
hugh.conlon@pfizer.com

[1] Analytical Research and Development, Biotherapeutics Pharmaceutical Sciences, Pfizer Inc., Chesterfield, MO 63017, USA

[2] Analytical Research and Development, Biotherapeutics Pharmaceutical Sciences, Pfizer Inc., Andover, MA 01810, USA

[3] UCB Pharma, Bainbridge Island, WA 98110, USA

1 Introduction

An increasing number of biosimilars are available in major global markets, due to increased biopharmaceutical industry interest over the last decade, with more than ten biosimilars approved in the USA, more than 29 approved in Europe, and dozens currently in developmental pipelines [1]. The abbreviated biosimilars approval pathway relies heavily on a comprehensive demonstration of similarity to the reference product (originator) using routine and heightened analytical characterization methods [2].

During development of a candidate biosimilar, routine product quality testing is supplemented with heightened analytical characterization to evaluate similarity to the reference

product. Heightened analytical characterization generally leverages state-of-the-art methods and can be orthogonal to more routine methods, such as high-performance liquid chromatography (HPLC)- and capillary electrophoresis-based techniques. Through characterization, improved knowledge is acquired of not only the biosimilar candidate, but also of the reference product, creating opportunities to better understand the therapeutic mechanisms of action and degradation pathway(s). This knowledge benefits the design, development, stability, and efficacy of future biotherapeutics.

Infliximab is a mouse/human chimeric IgG1 monoclonal antibody prescribed for the treatment of Crohn's disease, psoriasis, rheumatoid arthritis, and other autoimmune diseases [3, 4]. Infliximab functions by binding to the inflammation-regulating cytokine, tumor necrosis factor (TNF), and inhibiting receptor interactions, thereby decreasing inflammation and autoimmune response in patients [5]. The structural basis for TNF neutralization by infliximab was revealed previously in the crystal structure of the TNF trimer in complex with the infliximab Fab (fragment antigen binding) fragment [6]. Biosimilar versions of infliximab have been approved in the USA (Ixifi™ [Pfizer, USA], Inflectra® [Pfizer, USA]) and Europe (Zessly® [Sandoz, Germany], Inflectra®/Remsima™ [Celltrion, South Korea], Flixabi® [Biogen, USA]).

The development of PF-06438179/GP1111 (Ixifi™/Zessly®) involved analytical similarity assessments that leveraged state-of-the-art characterization techniques to demonstrate similarity in primary and higher order structure (HOS), post-translational modifications (PTMs), purity, and potency [7]. With the inextricable relationship between molecular structure and biological function, it is well-recognized that biosimilarity depends closely on molecular structure, which can be elucidated using established biophysical methods, such as circular dichroism, Fourier Transform Infrared (FT-IR), and Raman and intrinsic fluorescence spectroscopies. These spectroscopic methods enable routine structural evaluation of bio-molecules with a relatively low resource burden, but are limited in sensitivity to detect small conformational changes that might impact function [8]. In contrast, heightened structure characterization methods, including X-ray crystallography, two-dimensional nuclear magnetic resonance (2D NMR), and hydrogen-deuterium exchange analyzed by mass spectrometry (HDX-MS), require more resources than established methods, but generally offer greater sensitivity to detect local structural changes. X-ray crystallography, in particular the crystallization process, is sensitive to heterogeneity in multiple relevant quality attributes, including primary structure, HOS, PTMs, and purity [9]. The resulting structures enable molecular comparisons at unprecedented levels of detail, relative to more routine spectroscopic techniques. We previously reported the crystal structures of the infliximab Fab and Fc (fragment crystallizable) fragments, sourced from Remicade® obtained from the US market [10]. The structures, along with supportive biochemical and biophysical assessments, revealed a Fab domain-mediated self-association mechanism, which was not readily apparent in the earlier Fab:TNF complex structure [6].

In the current study, we determined crystal structures of the PF-06438179/GP1111 Fab and Fc fragments, each in two distinct crystal forms. The structures represent the first detailed structural description for an approved monoclonal antibody biosimilar. The Fc structures give insight into the core N-linked glycan structure and are consistent with biochemical evaluation of the glycoforms. The Fab and Fc structures further support structural similarity of PF-06438179/GP1111 to the originator infliximab. Lastly, we confirm using analytical ultracentrifugation (AUC) that the self-association interface observed in the Fab crystal structures conveys self-association in solution, similar to the originator. The high-resolution structures demonstrate that the specific regions responsible for infliximab mechanisms of action (e.g., complementarity-determining regions [CDRs] and N-linked glycans) and physical properties (e.g., reversible self-association interface) are structurally indistinguishable between PF-06438179/GP1111 and the reference product.

2 Materials and Methods

2.1 Materials

One hundred milligram drug product vials of PF-06438179/GP1111 and Remicade® were reconstituted in 2.5 mL of sterile water for injection (Hospira) to a concentration of 40 mg/mL.

2.2 Papain Digestion and Fragment Purification

30 mg of infliximab was digested with immobilized papain slurry (Pierce #20341) for 5 h at 37 °C, using a 1:60 ratio of enzyme to antibody. Enzyme activation was performed following the manufacturer's instructions. The Fab fragment was separated from the Fc fragment using MabSelect Protein A affinity chromatography (GE Life Sciences, Marlborough, MA, USA), and both fragments were purified further by size-exclusion HPLC using a YMC-Pack Diol-200 column (Waters, Milford, MA, USA). Samples were concentrated to 10 mg/mL in succinate 20 mmol/L, sodium chloride 150 mmol/L, pH 6, and frozen prior to crystallization and analysis by AUC–sedimentation velocity (AUC-SV).

2.3 Crystallization, Data Collection, and Structure Determination

Crystals of the infliximab Fab fragment were obtained in I-centered orthorhombic ($I2_12_12_1$) and C-centered orthorhombic ($C222_1$) crystal forms. Crystals in the $I2_12_12_1$ form were grown in sodium malonate 2.16 M and 4% t-butanol and were cryo-protected with 20% v/v ethylene glycol prior to data collection. Crystals of the US- and European Union (EU)-sourced Remicade® Fab fragments were grown in the presence of nicotinamide adenine dinucleotide (NAD) 10 mmol/L and 4% pentaerythriol ethoxylate, in place of t-butanol, respectively. Crystals in the $C222_1$ form were grown in 19.5% w/v polyethylene glycol (PEG) 10,000 and 4-(2-hydroxyethyl)-1-piperazineethanesulfonic acid (HEPES) 0.1 M at pH 7.8 (or as described previously [10]) and were cryo-protected with 20% v/v ethylene glycol prior to data collection.

Crystals of the infliximab Fc fragment were obtained in $C222_1$ and P-centered orthorhombic ($P2_12_12_1$) crystal forms. Crystals in the $C222_1$ form were grown in 4–10% v/v isopropanol, zinc acetate 0.2 M, and sodium cacodylate 0.1 M at pH 6.5–6.8, and were cryo-protected with 20% v/v ethylene glycol prior to data collection. Crystals in the $P2_12_12_1$ form were grown in 20% PEG 3350 and potassium nitrate 0.2 M and were cryo-protected with 20% v/v ethylene glycol prior to data collection.

Crystals were harvested, and complete X-ray datasets were obtained at the Advanced Photon Source (APS), Life Sciences Collaborative Access Team (LS-CAT) beamline sector 21. Fab crystals diffracted X-rays to 2.15 and 1.95 Å resolution for $I2_12_12_1$ and $C222_1$ crystal forms, respectively. Fab crystal structures were solved by molecular replacement in Phaser MR [18] using the constant and variable domains of the infliximab Fab from Protein Data Bank (PDB) ID 4G3Y [6] as independent search models. All structures were refined in Phenix [19] with manual model building in Coot [20]. Structures were validated with MolProbity [21]. Data collection and refinement statistics for the $I2_12_12_1$ and $C222_1$ crystal forms are shown in Table 1.

Fc crystals diffracted X-rays to 2.0 and 2.1 Å resolution for $C222_1$ and $P2_12_12_1$ crystal forms, respectively. The crystal structures were solved by molecular replacement in Phaser MR using individual immunoglobulin domains derived from PDB ID 4CDH [22] as search models (100% sequence identity). The Fc crystal structure was refined in Phenix with automated model building in ARPw/ARP (European Molecular Biology Laboratory; https://www.embl-hamburg.de/ARP/), manual model building in Coot, and was validated with MolProbity (Duke Biochemistry; http://molprobity.biochem.duke.edu/). Data collection and refinement statistics are shown in Table 1. Structure figures were generated using the PyMOL Molecular Graphics System (Schrödinger, LLC, New York, NY, USA).

Coordinates and structure factors have been deposited in the RCSB PDB (http://www.rcsb.org/pdb/) under accession codes 6UGS, 6UGT, 6UGU, 6UGV, 6UGW, 6UGX, and 6UGY.

2.4 Determination of *N*-glycan Content by Hydrophilic Interaction Liquid Chromatography (HILIC)

N-linked glycans were released using PNGaseF (Prozyme GKE-5006B), labeled with 2-AB/1 M sodium cyanoborohydride 0.35 M solution, and analyzed by a hydrophilic interaction chromatography gradient using a Waters Xbridge™ amide column, 3.5 µm, 4.6 × 150 mm and a Waters 2695 HPLC with fluorescence detection (excitation at 330 nm and emission at 420 nm).

2.5 Analytical Ultracentrifugation–Sedimentation Velocity

Samples were diluted to 0.1, 0.3, and 0.6 mg/mL with sodium phosphate 20 mmol/L, sodium chloride 400 mmol/L, pH 7.2. Samples were run in triplicate using 1.2 cm centerpieces in a Beckman Coulter Analytical Ultracentrifuge Proteome XL/I (Beckman Coulter, Indianapolis, IN, USA) at 45,000 rotations per minute (RPM) at 20 °C. One hundred scans were collected at a wavelength of 280 nm. Data were analyzed using Sedfit (version 14.1) [23] to generate c(s) size distribution plots and to determine the relative abundance of the various species. Sednterp (version 20130813 BETA) was used to determine partial specific volumes, as well as the solvent viscosity and density. Partial specific volumes of 0.725 and 0.729 mL/g were used for the Fab and Fc fragments, respectively, based on their amino acid compositions. A solvent density of 1.017 g/mL and a solvent viscosity of 1.05 cP were used for data analysis.

3 Results

3.1 PF-06438179/GP1111 Crystal Structures

The physicochemical and functional similarity of PF-06438179/GP1111 to Remicade® has been established through a robust analytical similarity assessment [7]. To further characterize the HOS of this biosimilar, we determined crystal structures of the Fab and Fc fragments of PF-06438179/GP1111 as well as Remicade® sourced from the US and EU markets. The antibody was digested with papain and the purified Fab and Fc fragments were crystallized. Crystal structures were determined using molecular replacement methods and the final refinement statistics are shown in Table 1. All structures are of high quality for the resolution of their data, as determined by MolProbity

Table 1 Crystallographic data collection and refinement statistics

	Overall (highest shell)	Overall (highest shell)	Overall (highest shell)	Overall (highest shell)
Infliximab fragment	Fab	Fab	Fc	Fc
Crystallization conditions	Sodium malonate 2.16 M, 4% t-butanol (cryo: 20% EG)	HEPES 0.1 M pH 7.8, 19.5% PEG 10,000 (cryo: 20% EG)	10% isopropanol, zinc acetate 0.2 M, sodium cacodylate 0.1 M pH 6.5 (cryo: 20% EG)	20% PEG 3350, potassium nitrate 0.2 M (cryo: 20% EG)
Beam line	APS LS-CAT 21 ID-G	APS LS-CAT 21 ID-F	APS LS-CAT 21 ID-G	APS LS-CAT 21 ID-F
Δϕ(°)	1.0	1.0	1.0	1.0
Images	150 (150°)	200 (200°)	150 (150°)	200 (200°)
Exposure (s)	1	1	1	1
Detector distance (mm)	200	190	245	170
Wavelength (Å)	0.97872	0.97856	0.97872	0.97856
Space group	$I2_12_12_1$	$C222_1$	$C222_1$	$P2_12_12_1$
Unit cell	$a=90.60$ Å, $b=93.33$ Å, $c=316.56$ Å; $\alpha=\beta=\gamma=90°$	$a=87.21$ Å, $b=139.09$ Å, $c=195.68$ Å; $\alpha=\beta=\gamma=90°$	$a=50.09$ Å, $b=148.09$ Å, $c=75.79$ Å; $\alpha=\beta=\gamma=90°$	$a=49.40$ Å, $b=74.61$ Å, $c=149.09$ Å; $\alpha=\beta=\gamma=90°$
Solvent content (%)	66	60	50.5	56.7
V_m (Å^3/Da)	3.60	3.10	2.48	2.84
Resolution (Å)	50–2.15 (2.21–2.15)	50–1.95 (2.00–1.95)	50–2.0 (2.05–2.00)	50–2.1 (2.15–2.10)
I/σ	10.74 (3.08)	15.61 (3.53)	13.69 (3.69)	13.68 (3.75)
Completeness (%)	99.1 (98.7)	99.9 (100)	99.9 (100)	99.8 (100)
R_{merge}	0.108 (0.565)	0.077 (0.491)	0.083 (0.497)	0.094 (0.499)
CC ½	99.4 (78.8)	99.8 (92.1)	99.8 (88.3)	99.7 (88.5)
Multiplicity	4.9 (5.1)	6.2 (6.3)	6.1 (6.2)	6.0 (6.1)
Reflections	72,719 (5315)	86,561 (6356)	19,460 (1417)	32,975 (2430)
Mosaicity	0.2	0.4	0.2	0.5–0.8
Refinement				
R	0.155 (0.235)	0.161 (0.227)	0.182 (0.211)	0.201 (0.235)
R_{free}	0.210 (0.295)	0.198 (0.277)	0.219 (0.280)	0.256 (0.322)
FOM	0.84	0.87	0.85	0.82
Coordinate error (Å)	0.23	0.19	0.19	0.28
Wilson B-factor (Å^2)	26.7	23.6	27.6	26.0
Validation				
Ramachandran favored (%)	97.33	97.8	99.51	99.8
Ramachandran outliers (%)	0	0.12	0	0
Rotamer outliers (%)	1.34	0.95	1.10	1.9
Clash score	2.63 (99th percentile)	1.02 (100th percentile)	3.30 (99th percentile)	1.92 (100th percentile)
Molprobity score	1.27 (100th percentile)	0.85 (100th percentile)	1.15 (100th percentile)	1.16 (100th percentile)

APS LS-CAT Advanced Photon Source Life Sciences Collaborative Access Team, $C222_1$ C-centered orthorhombic, *CC* correlation coefficient, *EG* ethylene glycol, *Fab* fragment antigen binding, *Fc* fragment crystallizable, *FOM* figure of merit, *HEPES* 4-(2-hydroxyethyl)-1-piperazineethanesulfonic acid, $I2_12_12_1$ I-centered orthorhombic, $P2_12_12_1$ P-centered orthorhombic, V_m Matthews coefficient

scores (Table 1 for PF-06438179/GP1111, Electronic Supplementary Material [ESM] Table S1 for Remicade®-EU and previously reported for Remicade®-US [10]).

Fc structures of PF-06438179/GP1111 were determined in $C222_1$ and $P2_12_12_1$ crystal forms at 2.0 and 2.1 Å resolution, respectively (Fig. 1a). The asymmetric unit of the $C222_1$ form contained one Fc chain, and the second Fc chain of the biological dimer was related via crystallographic symmetry. The $P2_12_12_1$ form contained two chains, representing the complete biological dimer, in the asymmetric unit. Structural alignment of the two crystal forms reveals a small, ~ 9 ° rotation of the C_H3 domain relative to the C_H2 domain, consistent with flexibility between the Fc subdomains. Within the C_H2 and C_H3 domains, however, the structures are highly conserved, with all-atom root-mean-squared deviations (RMSDs) of 0.90 and 0.91 Å, respectively, after least squares (LSQ) alignment. In the $C222_1$ crystal form, electron density corresponding to zinc ions from the crystallization buffer

was observed. One of the zinc ions is positioned at the C_H2/C_H3 domain interface (Fig. 1a, inset), coordinated by His_{313} (C_H2), His_{438} (C_H3), a water molecule, and an acetate ion (also from the crystallization buffer). Similar coordination of zinc ions in the C_H2/C_H3 interface has been observed previously [11, 12] and was proposed to stabilize a more open conformation between the C_H2 domains of the Fc dimer. The $P2_12_12_1$ Fc crystals were grown in the absence of zinc, and Zn^{2+} atoms are not observed in the resulting $P2_12_12_1$ crystal form structure. When comparing the two crystal forms, average Cα atom *B*-factors for the PF-06438179/GP1111 C_H2/C_H3 hinge (residues 342–347) are lower in the Zn^{2+}-bound $C222_1$ form (19.9 $Å^2$) than in the $P2_12_12_1$ form (32.7 $Å^2$), indicating that Zn^{2+} coordination in this position imposes some rigidity to the Fc domain, while crystal packing interactions likely stabilize the overall conformation observed in each crystal form. Although it has been reported that Zn^{2+} can affect binding of Fc receptors [12], the absence of Zn^{2+} in the $P2_12_12_1$ structure indicates that the zinc acetate 0.2 M used to crystallize the $C222_1$ form was the source of the zinc ions observed in that structure.

Based on related crystal structures such as PDB ID 4CDH, we built the *N*-linked glycan into the well-resolved omit maps' (|Fo|-|Fc|) positive difference density (ESM Fig. S1). Determination of the PF-06438179/GP1111 glycan content (Fig. 1b) demonstrates that G0F, G1Fa, and G1Fb are the most abundant glycans on PF-06438179/GP1111, with combined levels totaling ~ 85%. In the crystal structures, the glycan anchored to Asn_{300} corresponds to the G1F minus *N*-acetyl glucosamine (GlcNAc) in the $C222_1$ crystal form and to G0F in the $P2_12_12_1$ form (Fig. 1c). In both Fc crystal structures, the electron density corresponding to the fucose and terminal GlcNAc or galactose is the least ordered, indicating flexibility among the terminal sugar residues (ESM Fig. S1). Combining the observations from both crystal forms, the structures are consistent with the presence of

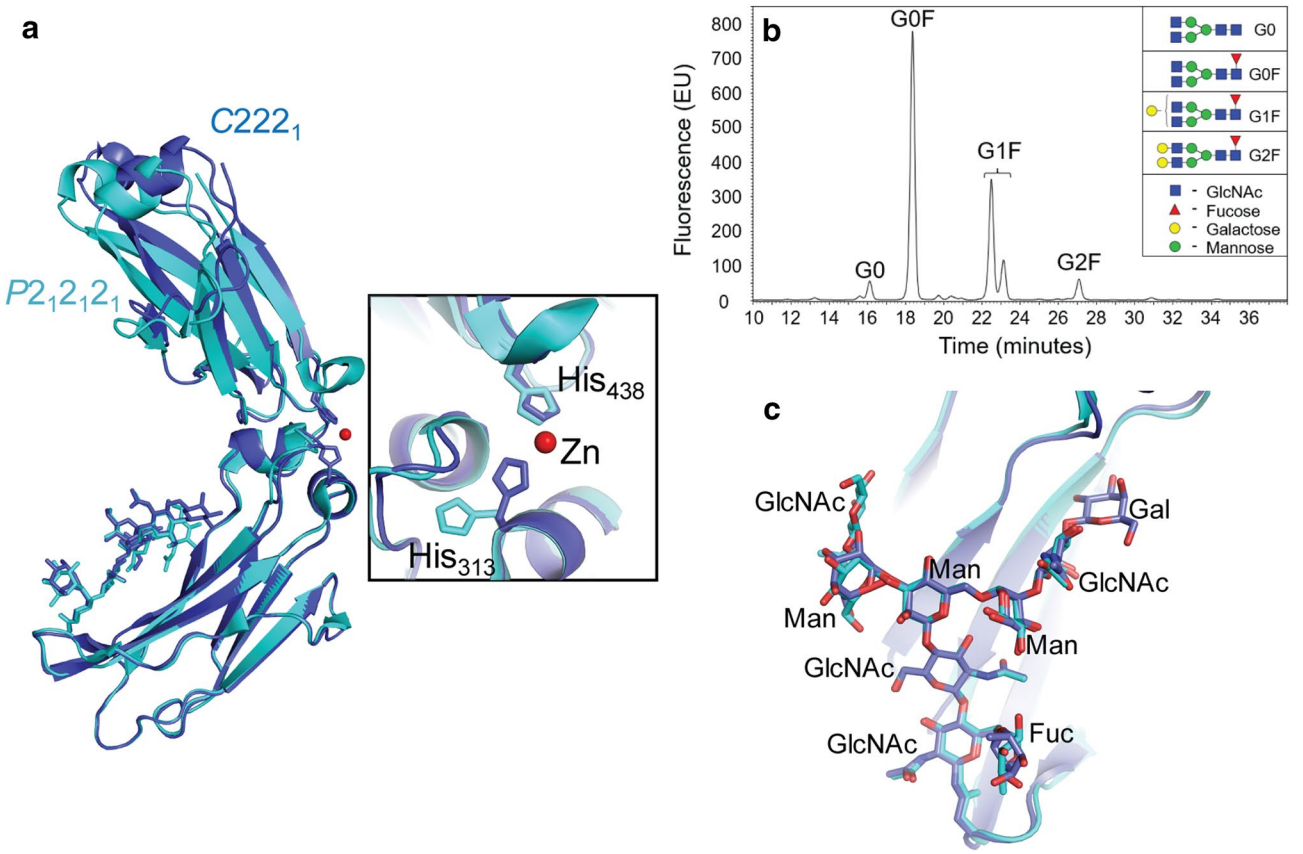

Fig. 1 **a** Crystal structures of the PF-06438179/GP1111 Fc fragment in C-centered orthorhombic ($C222_1$; blue) and P-centered orthorhombic ($P2_12_12_1$; cyan) crystal forms. *N*-linked glycans are shown in stick representation. A ~ 9 ° rotation between the C_H2 and C_H3 domains was observed between the two forms, with His_{438} and His_{313} coordinating a Zn atom at the C_H2/C_H3 interface in the more open $C222_1$ form (inset). **b** Released *N*-glycan analysis using hydrophilic interaction liquid chromatography (HILIC) demonstrates that the most abundant glycans on PF-06438179/GP1111 are G0F and G1F. **c** A structural overlay of the glycans resolved in the $C222_1$ (blue, corresponding to G1F minus GlcNAc) and $P2_12_12_1$ (cyan, corresponding to G0F) forms. Combined, the structures are consistent with the presence of G1F, with weak electron density around terminal sugar residues consistent with flexibility and/or high levels of G0F content. *EU* emission units, *Fuc* fucose, *Gal* galactose, *GlcNAc N*-acetyl glucosamine, *Man* mannose

G1F, although weak density around the terminal galactose residue (in the $C222_1$ form) and the abundance of G0F species shown chromatographically indicate that the crystal, like the intact antibody in solution, contains a mixture of G0F and G1F species. Furthermore, the terminal galactose residues in G1Fa or G1Fb glycoforms would not be sterically hindered in the crystal lattices of either crystal form, suggesting that one glycoform would not be expected to preferentially crystallize over another.

The $C222_1$ Fc fragment crystal form was also the basis for the assessment of structural similarity, as structures of Remicade® (sourced from the USA and EU) were also determined in this crystal form [10]. Crystallization conditions and unit cell parameters for these isomorphous Fc fragment crystals are compared in ESM Table S2. The overlaid cartoon representations of PF-06438179/GP1111 and Remicade® Fc fragment structures, shown in Fig. 2a, reveal a high degree of similarity between backbone structures. Additionally, the all-atom RMSD (including side-chains) between PF-06438179/GP1111 and US-sourced Remicade® is 0.47 Å and between PF-06438179/GP1111 and EU-sourced Remicade® is 0.45 Å. These values are essentially identical to the 0.43 Å all-atom RMSD between the US- and EU-sourced Remicade® Fc structures. In addition, the *N*-linked glycan structure of the biosimilar is fully consistent with that of the originator (Fig. 2b), despite production in Chinese hamster ovary (CHO) and SP2/0 cell lines, respectively.

Crystal structures of the PF-06438179/GP1111 Fab fragment were determined in two distinct crystal forms: in $I2_12_12_1$ at 2.15 Å resolution and in $C222_1$ at 1.95 Å resolution. Both crystal forms contain two Fab fragments in the asymmetric unit, and the Fab variable and constant regions are highly similar in both crystal forms. The all-atom RMSDs of the LSQ superposed crystal forms are 0.51–0.59 and 0.80–0.87 Å for the variable and constant regions, respectively. The structures are fully consistent with those determined previously of the infliximab Fab fragment

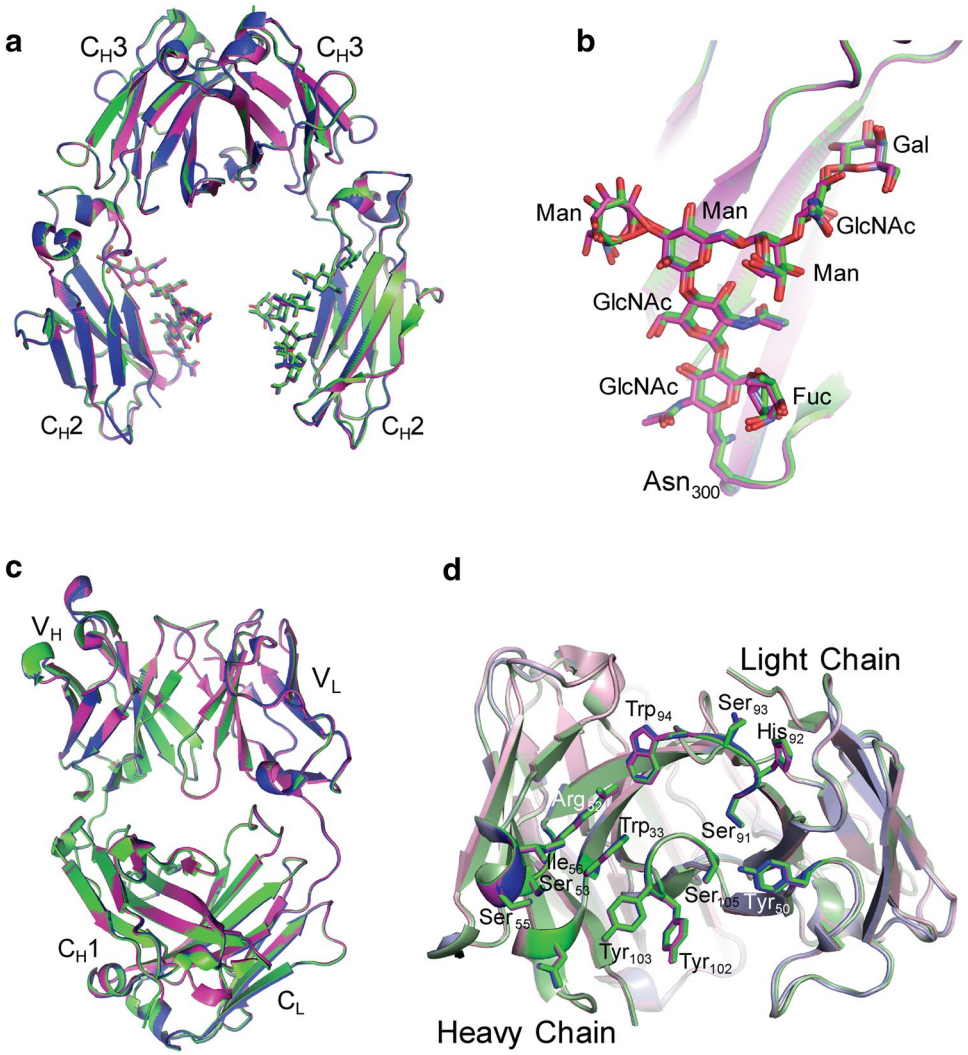

Fig. 2 PF-06438179/GP1111 structures (blue) are overlaid with structures determined from Remicade® sourced from the US (green) and EU (magenta) markets. **a** and **c** show the superposition of Fc and Fab fragments, respectively. *N*-linked glycans on the Fc fragment shown in stick representation and antibody subdomains (C_H1–C_H3, V_H, V_L, and C_L) are labeled. Superposition of N-linked glycans in the Fc fragment (**b**; sticks) and complementarity-determining region (CDR) loops in the Fab fragment (**d**) of PF-06438179/GP1111 and Remicade® demonstrate similar structural elements in regions specifically associated with the infliximab mechanisms of action. Oxygen atoms are colored red and nitrogen atoms are colored blue in **b**. Sticks in **d** show residues that contact the tumor necrosis factor (TNF) antigen upon binding. C_H constant region (heavy chain), C_L constant region (light chain), *Fuc* fucose, *Gal* galactose, *GlcNAc* N-acetyl glucosamine, *Man* mannose, V_H variable region (heavy chain), V_L variable region (light chain)

isolated from Remicade®-US [10] or Remicade®-EU (ESM information) and were used to demonstrate structural similarity between the biosimilar and originator. Crystallization conditions and unit cell parameters for the isomorphous Fab crystals used in the similarity assessments are compared in ESM Table S3. Figure 2c shows the overlaid Fab fragment structures from PF-06438179/GP1111 and from US- and EU-sourced Remicade®, and Fig. 2d shows the CDR loops with the residues that bind the TNF antigen as sticks [6]. The overlays demonstrate visually the high degree of similarity in the overall backbone conformation and among the antigen-binding residues. All-atom RMSD values for the two copies in the asymmetric unit were then compared between PF-06438179/GP1111 and US- and EU-sourced Remicade® for the $I2_12_12_1$ (Table 2) and $C222_1$ (Table 3) crystal forms. Tables 2 and 3 also show the mean B values (temperature factors) for the Fab structures. Within the asymmetric units of $I2_12_12_1$ and $C222_1$ crystals, the all-atom RMSD values between heavy chains (chains H and A) range from 0.35 to 0.46 Å and the all-atom RMSD values between light chains (chains L and B) range from 0.41 to 0.52 Å. These ranges, highlighted in bold in Tables 2 and 3, reflect differences within the same molecule (i.e., within the same crystal) when presented in the context of the non-symmetry related molecules within the crystal lattice. Thus, these could be viewed as the variability in conformation within the same lot. Comparing PF-06438179/GP1111 to Remicade® structures, all-atom RMSD values (italicized in Tables 2 and 3) range from 0.15 to 0.41 Å when comparing chain H or A, and 0.27 to 0.47 Å when comparing chain L or B. Comparing between Fab molecules (e.g., chain H vs. chain A or chain L vs. chain B) generally shows slightly higher RMSD values; however, all pairwise RMSD values are quite similar overall and support the conclusion that the PF-06438179/GP1111 Fab structure is indistinguishable from that of Remicade®.

3.2 Description of the Self-Association Interface on PF-06438179/GP1111

We previously demonstrated that a light chain:light chain interface facilitates self-association of infliximab, using

Table 2 All-atom root-mean-squared deviation values for Fab (fragment antigen binding) samples in the I-centered orthorhombic ($I2_12_12_1$) crystal form

Chain ID	Mean B (Å^2)	RMSD (Å)					
		Chain H PF-06438179/GP1111	Chain A PF-06438179/GP1111	Chain H Remicade®-US	Chain A Remicade®-US	Chain H Remicade®-EU	Chain A Remicade®-EU
Chain ID (heavy chain)							
PF-06438179/GP1111 chain H	31.91	–					
PF-06438179/GP1111 chain A	32.85	**0.414**	–				
Remicade®-US chain H	28.94	*0.333*	0.415	–			
Remicade®-US chain A	30.51	0.513	*0.405*	**0.353**	–		
Lot C chain H	32.20	*0.364*	0.412	*0.318*	0.447	–	
Lot C chain A	33.05	0.481	*0.344*	0.424	*0.405*	**0.412**	–
		Chain L PF-06438179/GP1111	Chain B PF-06438179/GP1111	Chain L Remicade®-US	Chain B Remicade®-US	Chain L Remicade®-EU	Chain B Remicade®-EU
Chain ID (light chain)							
PF-06438179/GP1111 chain L	33.59	–					
PF-06438179/ GP1111 chain B	32.61	**0.521**	–				
Remicade®-US chain L	30.61	*0.373*	0.512	–			
Remicade®-US chain B	29.88	0.542	*0.465*	**0.411**	–		
Remicade®-EU chain L	35.31	*0.422*	0.524	*0.393*	0.530	–	
Remicade®-EU chain B	35.63	0.536	*0.431*	0.475	*0.409*	**0.412**	–

Bold values reflect RMSDs within the same molecule (i.e., within the same crystal), representing variability within the same sample lot. Values were obtained from non-crystallographic symmetry related chains within the crystal lattice

Italic values represent RMSDs between the same chain in PF-06438179/GP1111 and Remicade® structures

EU European Union, *RMSD* root-mean-squared deviation

US-sourced Remicade® [10]. An identical interface was observed in the PF-06438179/GP1111 Fab crystal structures (Fig. 3) and Remicade® sourced from the EU market (not shown). Briefly, the asymmetric units of both $I2_12_12_1$ and $C222_1$ crystal forms contain two PF-06438179/GP1111 Fab fragments oriented in a head-to-tail fashion, forming a ~ 1050 Å^2 interface that occurs exclusively between the light chains (Fig. 3a, b). The interface area is larger than would be expected for crystal contacts, typically on the order of < 500 Å^2 [13], and is more aligned with the biological interface between the heavy and light chains (1617–1663 Å^2) or between the heavy chains of the Fc fragment (1010 Å^2). Although the specific light-chain:light-chain interactions are different, 25 interface residues are conserved between the two crystal forms (Fig. 3c), indicating that this region might facilitate self-association.

We and others have shown previously that concentration-dependent infliximab self-association is driven by the Fab domain [10, 14]. To confirm this phenomenon in PF-06438179/GP1111, AUC-SV analysis was performed on the Fab and Fc fragments at sample concentrations of 0.1, 0.3, and 0.6 mg/mL (Fig. 4). Consistent with the reference product, AUC-SV sedimentation coefficients for the Fc fragment were identical (3.61–3.62 S) at all concentrations, indicating that the Fc fragment does not undergo self-association under the sedimentation timescale at the concentrations tested. In contrast, the Fab fragment showed a concentration-dependent increase in the sedimentation coefficient, from 3.65 S at 0.1 mg/mL to 3.82 S at 0.3 mg/mL and 3.95 S at 0.6 mg/mL, indicative of relatively rapid self-association kinetics [15, 16]. At the highest concentration, the monomer–dimer equilibrium begins to resolve from the monomer in the c(s) distribution, where a shoulder corresponding to the monomer was observed (green profile in Fig. 4b). Additionally, AUC–sedimentation equilibrium (AUC-SE) analysis reveals the monomer–dimer equilibrium dissociation constant (K_D) to be 25 µmol/L, consistent with that of US-sourced Remicade® (21 µmol/L) and the EU-sourced Remicade® (23 µmol/L) (Lerch et al. [10] and ESM Fig. S2). Combined, the crystal structures and AUC studies demonstrate that, like the originator, PF-06438179/GP1111 self-association in the native state is driven by low-affinity Fab interactions that are reversible with fast kinetics.

Table 3 All-atom root-mean-squared deviation (RMSD) values for Fab (fragment antigen binding) samples in the C-centered orthorhombic ($C222_1$) crystal form

Chain ID	Mean B (Å^2)	RMSD (Å)					
		Chain H PF-06438179/GP1111	Chain A PF-06438179/GP1111	Chain H Remicade®-US	Chain A Remicade®-US	Chain H Remicade®-EU	Chain A Remicade®-EU
Chain ID (heavy chain)							
PF-06438179/GP1111 chain H	30.78	–					
PF-06438179/GP1111 chain A	31.00	**0.460**	–				
Remicade®-US chain H	25.84	*0.221*	0.483	–			
Remicade®-US chain A	26.17	0.425	*0.154*	**0.422**	–		
Remicade®-EU chain H	30.24	*0.202*	0.518	*0.255*	0.483	–	
Remicade®-EU chain A	30.00	0.412	*0.211*	0.426	*0.184*	**0.450**	–
		Chain L PF-06438179/GP1111	Chain B PF-06438179/GP1111	Chain L Remicade®-US	Chain B Remicade®-US	Chain L Remicade®-EU	Chain B Remicade®-EU
Chain ID (light chain)							
PF-06438179/GP1111 chain L	31.48	–					
PF-06438179/GP1111 chain B	28.86	**0.444**	–				
Remicade®-US chain L	25.99	*0.275*	0.561	–			
Remicade®-US chain B	24.98	0.405	*0.270*	**0.484**	–		
Remicade®-EU chain L	29.04	*0.342*	0.523	*0.281*	0.442	–	
Remicade®-EU chain B	27.34	0.436	*0.351*	0.463	*0.333*	**0.414**	–

Bold values reflect RMSDs within the same molecule (i.e., within the same crystal), representing variability within the same sample lot. Values were obtained from non-crystallographic symmetry related chains within the crystal lattice

Italic values represent RMSDs between the same chain in PF-06438179/GP1111 and Remicade® structures

EU European Union, *RMSD* root-mean-squared deviation

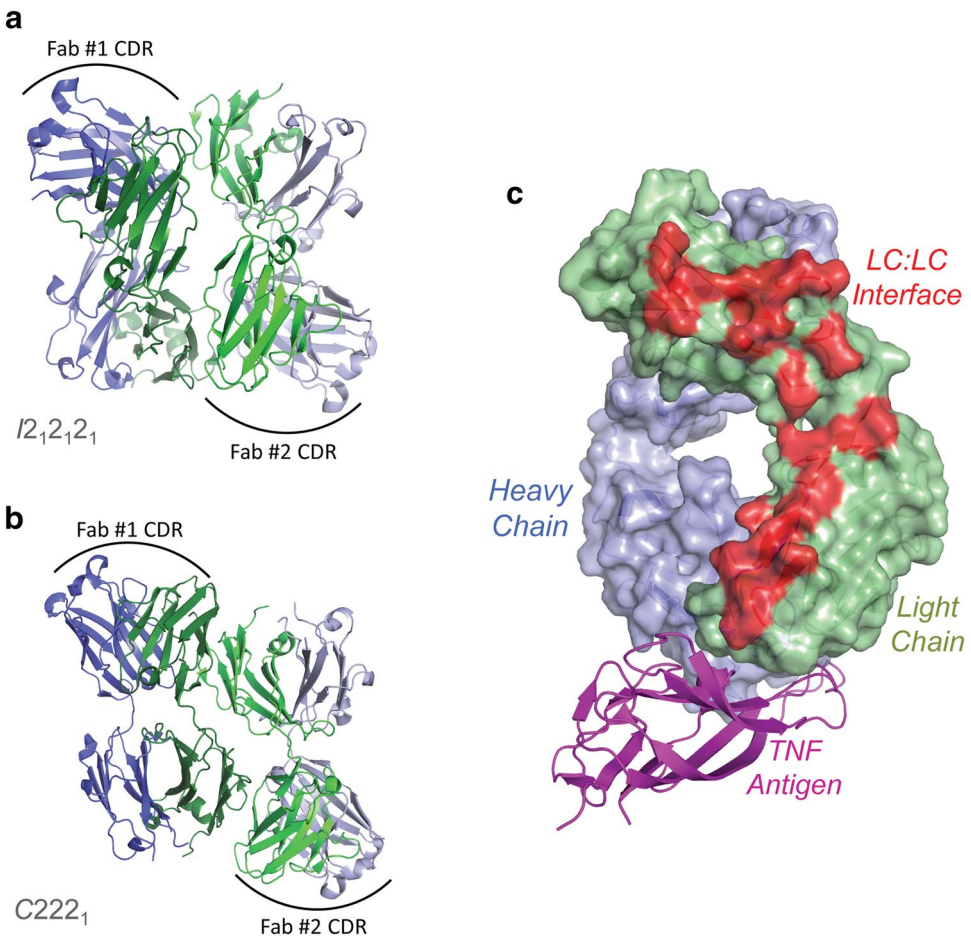

Fig. 3 PF-06438179/GP1111 Fab fragment crystals contain a putative dimer in the asymmetric unit. **a**, **b** Show the I-centered orthorhombic ($I2_12_12_1$) and C-centered orthorhombic ($C222_1$) crystal forms, respectively. Heavy chains are shown in shades of blue and light chains are shown in shades of green. Both putative dimers are positioned 'head-to-tail', as demonstrated by the relative complementarity-determining region (CDR) orientation indicated. The dimer interface in both crystal forms consists entirely of light chain:light (LC:LC) chain interactions. **c** A surface representation of the PF-06438179/GP1111 Fab fragment, with the heavy chain shown in blue, the light chain shown in green, and the 25 common residues that comprise the LC:LC interface in both crystal forms shown in red. The position of the tumor necrosis factor (TNF) antigen (magenta) from a superimposed structure of the Fab:antigen complex shows the relative positioning of the putative dimer interface and antigen binding region on the PF-06438179/GP1111 Fab fragment

4 Discussion

In the present study, crystal structures of the PF-06438179/GP1111 Fab and Fc fragments were determined in two crystal forms each. While relatively minor, differences between the Fc crystal forms are attributed to flexibility between the C_H2 and C_H3 domains, which is stabilized in the $C222_1$ form by coordination of a Zn atom by His_{313} and His_{438}. Combining the *N*-linked glycan observations in the two Fc crystal forms reveals the presence of G0F and G1F species, consistent with the major glycans identified by a quantitative assessment of enzymatically released glycans from the intact antibody in solution. The structures suggest that the core glycan structure is well-ordered with some flexibility among terminal sugar residues. The two Fab crystal forms also reveal flexibility between the variable and constant domains, as previously described [10].

Crystal structures of the Remicade® reference product, determined alongside the structures of PF-06438179/GP1111, enabled an assessment of structural similarity at near-atomic resolution. Global structural similarity was demonstrated by visually comparing the backbone representations of the PF-06438179/GP1111 and Remicade® structures, and more quantitatively by demonstrating low all-atom RMSD values between the structures. In contrast to most other structural or biochemical methods, X-ray crystallography also enables structural comparisons of localized regions, such as those known to affect the mechanisms of action. We have shown previously that the infliximab CDR loop structures are mostly rigid and that binding to the TNF antigen does not substantially affect their overall structure, including the side-chain positioning [10]. Here, we demonstrate that the PF-06438179/GP1111 CDR loop structure is indistinguishable from that

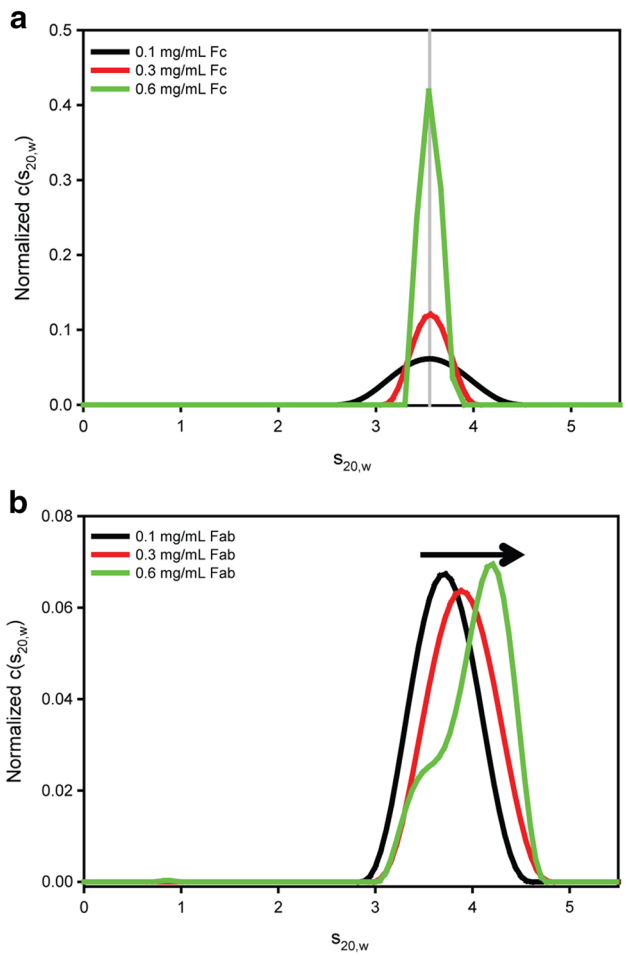

Fig. 4 Analytical ultracentrifugation–sedimentation velocity (AUC-SV) assessment of self-association in solution. The PF-06438179/GP1111 Fc fragment sedimentation coefficient is consistent at all measured concentrations (**a**), indicating that the Fc fragment does not self-associate in solution. In contrast, the Fab fragment exhibits increasing sedimentation coefficient values with concentration, indicative of reversible self-association (**b**)

of reference product Remicade® (Fig. 2d), which is consistent with highly similar binding affinities of both infliximab products for the soluble and transmembrane forms of the TNF antigen and similar potency as measured by inhibition of apoptosis and inhibition of endothelial–leukocyte adhesion molecule-1 (ELAM-1) expression [7].

While the main infliximab mechanisms of action depend primarily on Fab domain binding to TNF for blockade of TNF receptor binding and inhibition of the inflammatory cascade, antibody-dependent cellular cytotoxicity (ADCC) and complement-dependent cytotoxicity (CDC) of cells expressing the transmembrane form of TNF are plausible mechanisms of action for Crohn's disease and ulcerative colitis. Despite expression in different cell lines, the structures of the major N-linked glycans are highly similar between PF-06438179/GP1111 (produced in CHO cells) and Remicade® (produced in SP2/0 cells). The structural comparison of these regions known to influence effector functionality gives additional confidence that both infliximab molecules would have similar activity in the ADCC and CDC mechanisms of action [17].

Finally, we show that the PF-06438179/GP1111 light-chain drives Fab fragment self-association similar to that observed in Remicade® [10]. Of note, the light-chain:light-chain interface is distinct from the antigen binding site, as shown in the superposition of PF-06438179/GP1111 onto the TNF-bound Fab structure [6] (Fig. 3c). The non-overlapping nature of the sites indicates that, in solution, antibody concentration-dependent self-association would not be expected to affect antigen binding. Even when considering steric hindrance in a self-associated full-length antibody, the fast kinetics and overall low affinity of self-association (25 µmol/L) compared with a typical nM-pM antibody:antigen binding affinity make it unlikely that self-association would have a meaningful impact on TNF binding. In conclusion, while the overall demonstration of biosimilarity requires a wide array of analytical technologies, the PF-06438179/GP1111 crystal structures conclusively demonstrate that the specific regions associated with infliximab mechanisms of action are structurally indistinguishable from the reference product.

5 Conclusion

Protein HOS is critical for proper biotherapeutic function, where CDR loop structures and *N*-linked glycan structure/orientation, in part, govern therapeutic antibody mechanisms of action. While established spectroscopic methods typically reveal global structural information, X-ray crystallography enables structure elucidation of the functionally-relevant CDRs and *N*-linked glycans. The PF-06438179/GP1111 structures illustrate the capability of X-ray crystallography to bridge structural and functional assessments and contribute to the totality of evidence in the demonstration of biosimilarity.

Acknowledgements The authors thank Yin Luo and Eunhee Lee for their AUC-SE contributions to support this study. Stephen J. Mayclin and Thomas E. Edwards were employees of Beryllium Discovery Corp. (Bainbridge Island, WA 98110, USA) at the time that this study was conducted.

Compliance with Ethical Standards

Funding This study was sponsored by Pfizer Inc.

Conflict of interest Thomas F. Lerch, Penelope Sharpe, Hugh D. Conlon, Sharon Polleck, Jason C. Rouse, and Qin Zou are full-time employees and may be shareholders of Pfizer Inc. Stephen J. Mayclin and Thomas E. Edwards have no conflicts of interest to declare.

References

1. Kos IA, Azevedo VF, Neto DE, Kowalski SC. The biosimilars journey: current status and ongoing challenges. Drugs Context. 2018;7:212543. https://doi.org/10.7573/dic.212543.
2. Christl LA, Woodcock J, Kozlowski S. Biosimilars: the US regulatory framework. Annu Rev Med. 2017;68:243–54. https://doi.org/10.1146/annurev-med-051215-031022.
3. Gupta AK, Skinner AR. A review of the use of infliximab to manage cutaneous dermatoses. J Cutan Med Surg. 2004;8(2):77–89. https://doi.org/10.1007/s10227-004-0115-7.
4. Knight DM, Trinh H, Le J, Siegel S, Shealy D, McDonough M, et al. Construction and initial characterization of a mouse-human chimeric anti-TNF antibody. Mol Immunol. 1993;30(16):1443–53.
5. Maini RN, Feldmann M. How does infliximab work in rheumatoid arthritis? Arthritis Res. 2002;4(Suppl 2):S22–8.
6. Liang S, Dai J, Hou S, Su L, Zhang D, Guo H, et al. Structural basis for treating tumor necrosis factor alpha (TNFalpha)-associated diseases with the therapeutic antibody infliximab. J Biol Chem. 2013;288(19):13799–807. https://doi.org/10.1074/jbc.M112.433961.
7. European Medicines Agency, Committee for Medicinal Products for Human Use (CHMP) public assessment report—Zessly, 2018 May 30. https://www.ema.europa.eu/en/medicines/human/EPAR/zessly. Accessed 15 Jun 2019.
8. Weiss WFt, Gabrielson JP, Al-Azzam W, Chen G, Davis DL, Das TK, et al. Technical decision making with higher order structure data: perspectives on higher order structure characterization from the biopharmaceutical industry. J Pharm Sci. 2016;105(12):3465–70. https://doi.org/10.1016/j.xphs.2016.09.003.
9. Brader ML, Baker EN, Dunn MF, Laue TM, Carpenter JF. Using X-ray crystallography to simplify and accelerate biologics drug development. J Pharm Sci. 2017;106(2):477–94. https://doi.org/10.1016/j.xphs.2016.10.017.
10. Lerch TF, Sharpe P, Mayclin SJ, Edwards TE, Lee E, Conlon HD, et al. Infliximab crystal structures reveal insights into self-association. mAbs. 2017;9(5):874–83. https://doi.org/10.1080/19420862.2017.1320463.
11. Oganesyan V, Gao C, Shirinian L, Wu H, Dall'Acqua WF. Structural characterization of a human Fc fragment engineered for lack of effector functions. Acta Crystallogr D Biol Crystallogr. 2008;64(Pt 6):700–4. https://doi.org/10.1107/S0907444908007877.
12. Siberil S, Menez R, Jorieux S, de Romeuf C, Bourel D, Fridman WH, et al. Effect of zinc on human IgG1 and its FcgammaR interactions. Immunol Lett. 2012;143(1):60–9.
13. Rupp B. Biomolecular crystallography : principles, practice, and application to structural biology. New York: Garland Science; 2010.
14. Chen K, Long DS, Lute SC, Levy MJ, Brorson KA, Keire DA. Simple NMR methods for evaluating higher order structures of monoclonal antibody therapeutics with quinary structure. J Pharm Biomed Anal. 2016;128:398–407. https://doi.org/10.1016/j.jpba.2016.06.007.
15. Brown PH, Balbo A, Schuck P. Characterizing protein-protein interactions by sedimentation velocity analytical ultracentrifugation. Curr Protoc Immunol. 2008. https://doi.org/10.1002/0471142735.im1815s81 **(Chapter 18:Unit 18 5)**.
16. Howlett GJ, Minton AP, Rivas G. Analytical ultracentrifugation for the study of protein association and assembly. Curr Opin Chem Biol. 2006;10(5):430–6. https://doi.org/10.1016/j.cbpa.2006.08.017.
17. Raju TS. Terminal sugars of Fc glycans influence antibody effector functions of IgGs. Curr Opin Immunol. 2008;20(4):471–8. https://doi.org/10.1016/j.coi.2008.06.007.
18. McCoy AJ, Grosse-Kunstleve RW, Adams PD, Winn MD, Storoni LC, Read RJ. Phaser crystallographic software. J Appl Crystallogr. 2007;40(Pt 4):658–74. https://doi.org/10.1107/S0021889807021206.
19. Adams PD, Afonine PV, Bunkoczi G, Chen VB, Davis IW, Echols N, et al. PHENIX: a comprehensive Python-based system for macromolecular structure solution. Acta Crystallogr D Biol Crystallogr. 2010;66(Pt 2):213–21. https://doi.org/10.1107/S0907444909052925.
20. Emsley P, Lohkamp B, Scott WG, Cowtan K. Features and development of Coot. Acta Crystallogr D Biol Crystallogr. 2010;66(Pt 4):486–501. https://doi.org/10.1107/S0907444910007493.
21. Chen VB, Arendall WB 3rd, Headd JJ, Keedy DA, Immormino RM, Kapral GJ, et al. MolProbity: all-atom structure validation for macromolecular crystallography. Acta Crystallogr D Biol Crystallogr. 2010;66(Pt 1):12–21. https://doi.org/10.1107/S0907444909042073.
22. Silva-Martin N, Bartual SG, Ramirez-Aportela E, Chacon P, Park CG, Hermoso JA. Structural basis for selective recognition of endogenous and microbial polysaccharides by macrophage receptor SIGN-R1. Structure. 2014;22(11):1595–606. https://doi.org/10.1016/j.str.2014.09.001.
23. Schuck P. Size-distribution analysis of macromolecules by sedimentation velocity ultracentrifugation and lamm equation modeling. Biophys J. 2000;78(3):1606–19. https://doi.org/10.1016/S0006-3495(00)76713-0.